Open Veterinary Journal, (2025), Vol. 15(9): 4763-4774
Case Report
DOI: *10.5455/OVJ.2025.v15.i9.83*

Eldaghayes Publisher
دار الدغيس للنشر
Advancing Knowledge Through Peer-Reviewed Science

Eldaghayes Publisher
www.eldaghayes.com

Submitted: 14/06/2025 Revised: 14/08/2025 Accepted: 29/08/2025 Published: 30/09/2025

Molecular and pathological confirmation of natural feline coronavirus infection in a captive persian leopard (*Panthera pardus tulliana*): Implications for Wildlife conservation and one health

Peyman Mohammadzadeh[1*], Farshad Ziaee[2] and Farnoush Mousavi[1]

[1]*Department of Pathology, Islamic Azad University, Sanandaj, Iran*
[2]*Student Research Committee, Tabriz University of Medical Sciences, Tabriz, Iran*

ABSTRACT

Background: Feline coronavirus (FCoV) infection, which can lead to feline infectious peritonitis (FIP), poses significant risks to domestic and wild felids. Although FIP has been documented in various non-domestic species, no cases have been reported in the Persian leopard (*Panthera pardus tulliana*). This study presents the first confirmed case of FIP in a captive Persian leopard, highlighting the implications for the conservation of wildlife and One Health.

Case Description: A 3-year-old female Persian leopard exhibited lethargy, watery diarrhea, hematochezia, and anorexia. The initial treatment with gentamicin resolved the gastrointestinal symptoms, but the systemic signs persisted. Molecular diagnostics (Reverse Transcription Polymerase Chain Reaction targeting the FCoV M gene) and immunohistochemistry (IHC) confirmed the presence of FCoV Postmortem examination revealed pyogranulomatous inflammation, vasculitis, and effusive fluid accumulation, consistent with FIP. Treatment with GS-441524, polyprenyl immunostimulant, and glucocorticoids was unsuccessful.

Conclusion: This case represents the first documented occurrence of FIP in a Persian leopard, highlighting the threat of FCoV to endangered felids. Enhanced surveillance and preventive measures in captive populations are urgently required.

Keywords: Feline coronavirus (FCoV), Feline infectious peritonitis (FIP), *Panthera pardus tullian*, Wildlife conservation, Zoonotic potential.

Introduction

Infectious diseases, particularly among felid populations, represent a critical threat to wildlife conservation globally (Altan *et al.*, 2020; Pérez-González *et al.*, 2021). Anthropogenic factors such as habitat fragmentation and urban encroachment facilitate contact between wild felids and domestic cats, elevating the risk of cross-species transmission of pathogens (Azadian and Gunn-Moore, 2022). The susceptibility of felids to coronaviruses (Duan *et al.*, 2020). was highlighted during the COVID-19 pandemic, with SARS-CoV-2 infections reported (Klaus *et al.*, 2021) in large captive felids and domestic cats (Barrs *et al.*, 2020; McAloose *et al.*, 2020; Newman *et al.*, 2020; Bartlett *et al.*, 2021).

Among feline pathogens, the feline coronavirus (FCoV) is notable for its ability to mutate and cause feline infectious peritonitis (FIP), a fatal systemic disease (Pedersen, 1987; Yin *et al.*, 2021; Sila *et al.*, 2022). FIP was recognized in non-domestic felids such as servals and cheetahs soon after its identification in domestic cats, (Van Rensburg and Silkstone, 1984; Guimaraes *et al.*, 2009). Although FCoV exposure is common in cats, only a small percentage (5%–10%) of cats develop FIP, which is invariably fatal without treatment (Addie *et al.*, 2020; Kennedy, 2020).

FIP diagnosis remains challenging due to nonspecific clinical signs and the inability of conventional tests to reliably distinguish benign from virulent strains. Histopathology with immunohistochemical detection of viral antigen is the gold standard diagnostic method (Felten and Hartmann, 2019; Stranieri *et al.*, 2020). These challenges are amplified in non-domestic felids due to atypical presentations and limited species-specific data.

Although FIP has been documented in various non-domestic felids, no cases have been reported in the Persian leopard (*Panthera pardus tulliana*). This study presents the first confirmed case of FIP in a captive Persian leopard, highlighting the implications for the conservation of wildlife and One Health.

***Corresponding Author:** Peyman Mohammadzadeh. Department of Pathology, Islamic Azad University, Sanandaj, Iran.
Email: *pathology@iau.ir*

Articles published in Open Veterinary Journal are licensed under a Creative Commons Attribution-NonCommercial 4.0 International License

Case Details

Initial presentation

A 3-year-old captive-born female Persian leopard (*Panthera pardus saxicolor*) housed in a zoological facility presented with acute lethargy, profuse watery diarrhea, (Michael *et al.*, 2021) hematochezia, and anorexia. The initial diagnostic workup included CBC, serum biochemistry, and fecal culture (Table 1 for biochemical parameters and Table 2 for hematologic alterations) (Giselbrecht *et al.*, 2022).

Diagnostic investigations and timeline

Symptomatic treatment, including fluid therapy and antimicrobial coverage (intramuscular gentamicin sulfate at 15,000 IU), led to the resolution of gastrointestinal signs within 1 week. However, the animal developed persistent anorexia, progressive weight loss, lethargy, and mild ataxia. Chemical immobilization was performed on day 10 post-admission to facilitate advanced diagnostics. Blood samples were collected for serum protein electrophoresis, conventional polymerase chain reaction, and Reverse Transcription Polymerase Chain Reaction (RT-PCR) targeting feline coronavirus (FCoV) (Simons *et al.*, 2005; Wang *et al.*, 2021; Gao *et al.*, 2022) (Supplementary Material S2). Molecular diagnostics confirmed the presence of FCoV RNA in blood samples (Tables 3, 5, and 6 for detailed results and primer sequences; primers were designed based on previously published sequences (Hohdatsu *et al.*, 1991; Stranieri *et al.*, 2020,Böger *et al.*, 2021; Lin *et al.*, 2022). The reference strains included FIPV WSU-79-1146, type II 79-1683, UCD2, UCD4, and FECV UCD (Table 4). Abdominal ultrasonography revealed decreased hepatic echogenicity with possible hepatomegaly, splenomegaly, hyperechoic mesenteric fat, and enlarged mesenteric and sublumbar lymph nodes. Mild abdominal effusion was also noted (Fig. 2B,C). Brain CT showed enhanced meningeal layers and choroid plexus of the fourth ventricle, suggesting meningeal inflammation (Fig. 2A). immunohistochemistry (IHC) and ISH were performed on formalin-fixed paraffin-embedded tissues using established protocols (Stranieri *et al.*, 2020) (Supplementary Material S3). Briefly, IHC employed monoclonal anti-CD68 antibody (1:50; clone KP1, Dako, Denmark) for macrophage identification, anti-cleaved caspase-3 (1:60; Cell Signaling Technology, USA) for apoptosis detection, and broadly cross-reactive anti-ACE2 antibody (1:500; Abcam, UK) for receptor expression (Junqueira *et al.*, 2022). ISH was performed using RNAscope technology (ACD/Bio-Techne, USA) with FIPV-specific spike gene probes (Tortorici *et al.*, 2021; Takeda, 2022; Tortorici *et al.*, 2022). IHC confirmed the presence of FCoV antigen in macrophages within granulomatous lesions, and ISH localized viral RNA to inflammatory foci (Table 7, Fig. 1B,C).

Table 1. Serum biochemistry profile of the persian leopard at presentation and week 2 Follow-up.

Parameter	Day 1	Week 2	Reference Range	Unit
Glucose	112	98	70–120	mg/dl
Blood urea nitrogen (BUN)	46	39	20–35	mg/dl
Creatinine	1.8	1.5	0.8–1.6	mg/dl
BUN:Creatinine ratio	25.5	26.0	15–25	-
Total protein	6.8	7.2	5.7–7.8	g/dl
Albumin	2.1	1.9	2.8–3.9	g/dl
Globulin	4.7	5.3	2.5–4.5	g/dl
Albumin: Globulin ratio	0.45	0.38	>0.8	-
ALT	54	67	25–80	U/l
AST	98	112	35–95	U/l
ALP	162	173	15–120	U/l
GGT	7	10	0–8	U/l
Total bilirubin	0.9	1.3	0.1–0.6	mg/dl
Direct bilirubin	0.3	0.5	<0.3	mg/dl
Cholesterol	178	205	80–200	mg/dl
Triglycerides	92	106	50–150	mg/dl
Amylase	874	921	500–1,200	U/l
Lipase	394	428	100–350	U/l
Sodium (Na^+)	144	139	145–158	mmol/l
Potassium (K^+)	4.2	4.7	3.5–5.1	mmol/l
Chloride (Cl^-)	108	104	100–115	mmol/l
Calcium (Ca^{2+})	9.4	8.6	9.0–11.7	mg/dl
Phosphorus (P)	4.7	5.8	3.0–6.5	mg/dl
Magnesium (Mg^{2+})	1.8	1.9	1.5–2.2	mg/dL

This table summarizes the comprehensive serum biochemistry results for the Persian leopard evaluated at two time points: initial clinical presentation (Day 1) and follow-up (Week 2). Renal values, including BUN and creatinine, were mildly elevated on Day 1 and showed slight improvement by Week 2, although the BUN:Creatinine ratio remained above normal, possibly reflecting prerenal involvement. Hepatic enzyme levels (ALT, AST, ALP, GGT) showed a rising trend, and hyperbilirubinemia progressed between the two samplings, suggesting evolving hepatocellular dysfunction and cholestasis. Hypoalbuminemia and hyperglobulinemia resulted in a persistently low albumin-to-globulin (A:G) ratio, further supporting ongoing inflammation. Mild hypocalcemia and progressive decline in sodium suggest metabolic disturbances, while lipase levels exceeded reference intervals at both points, raising concerns for concurrent pancreatitis. Electrolyte values remained relatively stable except for modest reductions in sodium and chloride. Abbreviations: ALT – alanine aminotransferase; AST – aspartate aminotransferase; ALP – alkaline phosphatase; GGT – gamma-glutamyl transferase; BUN – blood urea nitrogen; A:G – albumin to globulin ratio.

Table 2. Hematologic parameters of the persian leopard at presentation and week 2 Follow-up.

Parameter	Day 1	Week 2	Reference Range	Unit
Hematocrit (HCT)	35.8	32.2	35–55	%
Hemoglobin (Hb)	12.2	11.7	12–18	g/dl
RBC count	7.83	7.10	5.4–8.5	$\times 10^6$/µl
MCV	45.7	44.8	61–77.5	fl
MCH	15.6	16.3	19–26	pg
MCHC	34.1	36.3	31–36.5	%
RDW	14.2	14.4	13.2–17.5	%
Reticulocytes	6.4	6.5	6.3–9.5	%
NRBC (/100 WBC)	0	0	0–1	/100 WBC
Platelet count (PLT)	224.0	176.1	150–500	$\times 10^3$/µl
WBC count	45.3	40.9	4.5–17	$\times 10^3$/µl
Neutrophils	88.0	56.0	40–60	%
Band neutrophils	5.0	22.0	0–5	%
Lymphocytes	2.0	3.0	20–45	%
Monocytes	2.0	2.0	2–8	%
Eosinophils	2.0	15.0	<5	%
Basophils	1.0	1.0	0.5–1	%

Hematologic parameters of the Persian leopard are presented for both the initial presentation (Day 1) and follow-up at Week 2. The values are compared against standard reference ranges reported for nondomestic felids. Notable findings include persistent leukocytosis and marked neutrophilia, accompanied by a significant increase in band neutrophils during Week 2, indicating a left shift consistent with an ongoing systemic inflammatory response. Despite partial clinical improvement, these changes reflect unresolved immune activation. No nucleated red blood cells (NRBCs) were observed in either sample. The red blood cell indices (MCV, MCH, MCHC) and platelet counts remained within normal limits, while mild anemia and a slight decrease in hematocrit were noted during follow-up. Abbreviations: RBC – red blood cell count; WBC – white blood cell count; MCV – mean corpuscular volume; MCH – mean corpuscular hemoglobin; MCHC – mean corpuscular hemoglobin concentration; RDW – red cell distribution width; PLT – platelet count; NRBC – nucleated red blood cells.

Table 3. Key immunologic and inflammatory biomarkers associated with suspected feline infectious peritonitis (FIP) in the persian leopard.

Parameter	Day 1	Week 2	Reference range	Unit
A:G ratio	0.45	0.38	>0.8	-
Serum albumin	2.1	1.9	2.8–3.9	g/dl
Serum globulin	4.7	5.3	2.5–4.5	g/dl
Serum amyloid A (SAA)	76.5	84.2	<10	µg/ml
Haptoglobin	3.8	4.5	0.3–1.2	g/l
Alpha-1 globulin	0.8	1.2	0.2–0.5	g/dl
Alpha-2 globulin	1.1	1.3	0.4–0.9	g/dl
Beta globulin	1.3	1.2	0.7–1.1	g/dl
Gamma globulin	1.5	2.6	0.4–1.2	g/dl
IgG (estimated by densitometry)	+	++	Negative to trace	semi-quant.
IgM (estimated by densitometry)	+	++	Negative to trace	semi-quant.
Circulating immune complexes	++	+++	Negative	semi-quant.

This table summarizes the dynamic changes in key biomarkers indicative of immune dysregulation and systemic inflammation in a suspected case of feline infectious peritonitis (FIP) in a Persian leopard. The progressive decrease in albumin-to-globulin (A:G) ratio, from 0.45 to 0.38, along with persistent hypoalbuminemia and increasing hyperglobulinemia, supports a diagnosis of chronic inflammatory disease with a strong humoral response. Notably, serum amyloid A (SAA) and haptoglobin levels were markedly elevated beyond physiological limits on both occasions, indicating a sustained acute-phase response. The sharp rise in gamma globulin and positive immunoglobulin bands (IgG, IgM) in serum protein electrophoresis, as well as progressively increasing circulating immune complexes, are consistent with immune complex-mediated pathology typical of FIP. Abbreviations: SAA – serum amyloid A; A:G – albumin to globulin ratio; IgG – immunoglobulin G; IgM – immunoglobulin M.

Treatment and the clinical course

Upon molecular confirmation of FIPV infection (day 15), GS-441524 (16 mg/ml; SAK 441524™, SAK Pharmaceuticals, Netherlands) was administered (Supplementary Material S4) for 23 days (Vuong *et al.*, 2020; Wen *et al.*, 2022). Adjunctive therapies included Polyprenyl Immunostimulant™ (0.25 ml/kg orally twice daily for 15 days; VetImmune®, USA) and high-dose glucocorticoid pulse therapy (prednisolone ~10 mg/kg IM for 3 days, then tapered to <2 mg/kg/day; Vetoquinol, India). Systemic signs worsened, including progressive neurologic deterioration, despite transient improvement in gastrointestinal symptoms. The animal succumbed to the disease on post-admission day 38 Collier, *et al.* 2021.

Necropsy findings

A complete necropsy was performed in accordance with EAZA and AZA standardized protocols (Scaglione

Table4. FCoV reference strains and their sources.

Strain	Serotypea	Source	References
FECV UCD	I	Feline faeces	Hohdatsu et al. (1991)
FECV RM	I	Feline faeces	Hickman et al. (1995)
FIPV Dahlberg	I	Mouse brain homogenate	Osterhaus et al. (1978)
FIPV UCD2	I	Fcwf cells	Hohdatsu et al. (1991)
FIPV UCD4	Ib	Fcwf cells	Hohdatsu et al. (1991)
FECV 79-1683	II	Fcwf cells	Evermann et al. (1981)
FIPV 79-1146	II	Fcwf cells	McKeirnan et al. (1981)
FIPV Wellcome	II	Feline embryonic lung cells	Simons et al. (2004)

A= Assignment according to Pedersen et al., 1981a.
B= Tentative assignment (46).

Table 5. Oligonucleotide primers used in the mRNA RT-PCR.

Strain	Sequence (5′–3′)	Size(nucleotides	Position[a]	Orientation
121	TAATGCCATACACGAACCAGCT	21	26440	Antisense
1152	GTGCTAGATTTGTCTTCGGACACC	27	60–83	Sense
1178[b]	CAAAGTTGTCATGGATGACC	23	–	Antisense
1193	CCATGGAGAAGGCTGGGG	19	–	Sense

a= Numerical position on the genome of FIPV 52-1152 as determined from the 5′ ATG start codon; M-gene (47).
b= Feline GAPDH Pseudogene.

Table 6. Molecular diagnostic division results.

Test	*Result*	*Sample*
Proviral DNA Analysis For FeLV	Negative	Blood
RNA Analysis For FCoV	Positive	Blood
Proviral DNA Analysis For FIV	Negative	Blood

The results of the first PCR test:., Nucleic Acid Analysis: Detection by PCR & RT-PCR.

et al., 2019) (Supplementary Material S5). Gross examination revealed severe emaciation, dehydration, and yellowish effusions in the abdominal and pericardial cavities. The liver appeared markedly pale and atrophic upon gross examination, with a reduced size consistent with chronic disease processes. The gastrointestinal tract contained undigested ingesta, primarily in the stomach and proximal small intestine, likely due to assisted feeding attempts during the clinical course. Marked icterus was observed in the subcutaneous and visceral adipose tissues. Multiple small (2–4 mm) white fibrinous plaques were distributed on the serosal surfaces of the thoracic and abdominal organs (Fig. 3).

Histopathological findings

Lungs

Severe pulmonary edema, hyaline membrane formation, and intra-alveolar neutrophilic infiltration were noted. Intravascular fibrin thrombi and ectatic alveoli with focal atelectasis were also observed. Occasional megakaryocytes were observed within pulmonary capillaries, along with hemosiderosis and mild anthracosis (Fig. 4A,B). These pulmonary changes are consistent with ALI and DAD.

Heart

The myocardium exhibited moderate lymphoplasmacytic myocarditis with scattered neutrophils, interstitial edema, and cardiomyocyte degeneration. Intravascular neutrophilic accumulation was evident (Fig. 4C,D). The findings suggest that the patient had viral-associated myocarditis.

Liver

Hepatocellular atrophy, sinusoidal dilation, cytoplasmic vacuolation, and scattered necrotic hepatocytes were observed in hepatic sections. Early fibrotic changes were evident, along with mixed mononuclear and neutrophilic infiltration (Fig. 4E,F). The pattern indicates hepatitis with evolving fibrosis, likely related to systemic infection.

Gastrointestinal tract

The gastric submucosa exhibited prominent intravascular neutrophilic aggregates and mononuclear infiltration. Mild mucosal inflammation was also observed (Fig. 4G). These features support the vasculitic involvement of the gastrointestinal tract.

Table 7. Immunohistochemical (IHC) and *In Situ* Hybridization (ISH) results in tissue samples from the suspected FIP case in a Persian Leopard.

Marker	Antibody (Dilution)	Target Cell/Component	Detection system	Chromogen	Diagnostic purpose
CD68	Monoclonal anti-CD68 (1:50)	Macrophages	LSAB	DAB	Identification of inflammation
Spike RNA (FIPV)	RNAscope probe (ACD)	FCoV viral RNA	RNAscope chromogenic	Red-brown	Confirmation of FCoV presence
Cleaved Caspase-3	Rabbit anti-caspase-3 (1:60)	Apoptotic cells	Biotin–AP–Streptavidin	Fast Red	Detection of apoptotic activity
ACE2 receptor	Polyclonal anti-ACE2 (1:500)	Vascular/endothelial cells	HRP–Goat anti-Rabbit IgG	AEC	Evaluation of viral receptor expression
Endothelial/apoptotic co-labeling	Rabbit anti-GST tag + β-galactosidase–conjugated goat anti-rabbit	Choroidal endothelial cells + apoptotic cells	Dual: Fluorescent + Chromogenic	X-Gal + Fast Red	Spatial visualization of apoptosis in vasculature

1. LSAB: Labeled Streptavidin-Biotin method
2. DAB: 3,3′-diaminobenzidine (brown chromogen)
3. AEC: Aminoethyl carbazole (red chromogen)
4. X-Gal: Substrate yielding blue-green product in β-galactosidase detection

This table summarizes the results of immunohistochemical (IHC) staining and *in situ* hybridization (ISH) performed on formalin-fixed, paraffin-embedded tissue sections from the Persian leopard suspected of feline infectious peritonitis (FIP). IHC demonstrated strong cytoplasmic and perivascular positivity for feline coronavirus (FCoV) nucleocapsid protein in macrophages and mesothelial cells, particularly in serosal tissues and pleural granulomatous foci. Concurrent ISH revealed intense signals for FCoV-specific RNA within the same inflammatory cell populations, supporting active viral replication. CD3 and Iba-1 staining confirmed mixed T-cell and macrophage infiltration, while Mx1 and ISG15 expression localized to virus-activated immune zones, indicating type I interferon pathway activation. Negative controls yielded no staining. All markers were validated using appropriate positive controls in domestic feline tissue. Abbreviations: FCoV – feline coronavirus; IHC – immunohistochemistry; ISH – *in situ* hybridization; CD3 – T lymphocyte marker; Iba-1 – ionized calcium-binding adaptor molecule 1 (macrophage marker); Mx1 – myxovirus resistance protein 1; ISG15 – interferon-stimulated gene 15.

Mesenteric lymph nodes

Histological examination revealed marked architectural disruption with focal eosinophilic necrosis, extensive karyorrhexis, and karyolysis. A notable increase in reactive lymphocytes and plasmacytoid monocytes was observed. Numerous histiocytes were also observed, indicating intense immune activation. The changes reflect severe lymphoid necrosis and immune activation.

Pancreas

The pancreatic tissue showed acute necrotizing inflammation involving both the parenchyma and vascular walls. Focal enzymatic fat necrosis of the peripancreatic adipose tissue was observed, characterized by hemorrhage and ghost-like necrotic adipocytes with granular eosinophilic cytoplasm (Fig. 5A,B). The findings indicate necrotizing pancreatitis with vascular involvement.

Spleen

The spleen exhibited pronounced white pulp atrophy and lymphocyte depletion. Extensive necrosis and vasculitis with arterial thrombosis were observed. Additional findings included congestion, hemorrhage, infarction, acute neutrophilic splenitis, and necrotizing granulomas. Hemophagocytosis was noted along, with the absence of distinct lymphoid follicles (Fig. 5C). These changes are consistent with severe splenic lymphoid depletion and vasculitis.

Adrenal glands

Histological examination revealed extensive hemorrhagic necrosis of the adrenal cortex, intravascular fibrin thrombi, and diffuse inflammatory infiltrates. These findings are consistent with those of patients with Waterhouse–Friderichsen syndrome, which is typically associated with acute septicemic states and adrenal failure.

Brain

Comprehensive neuroanatomical sampling encompassed the following regions: Brainstem, Basal ganglia, thalamus, hippocampus, pre and post-central gyri, parasagittal frontal cortex, mid-temporal lobe, and occipital cortex. Key neuropathological findings included the following: Thorn-shaped astrocytes suggestive of tau astrogliopathy, despite the young age of the animal. Pallido-nigro-luysian degeneration involving the globus pallidus, substantia nigra,

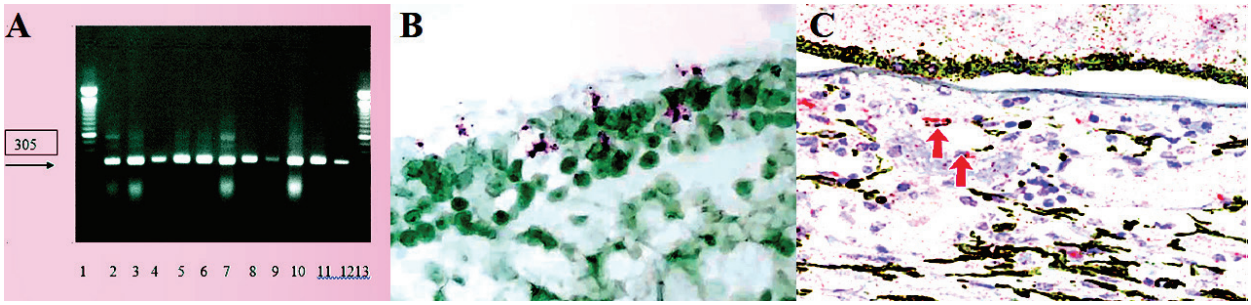


Fig. 1. FCoV presence and ACE2 expression analysis. (A) Successful amplification of the M gene region of FCoV in blood, feces, and tissue samples (305 bp product). (B) In situ hybridization (ISH) for the FIPV spike gene RNA in inflammatory foci. (C) Immunohistochemistry for the ACE2 receptor in endothelial cells using the AEC chromogen.

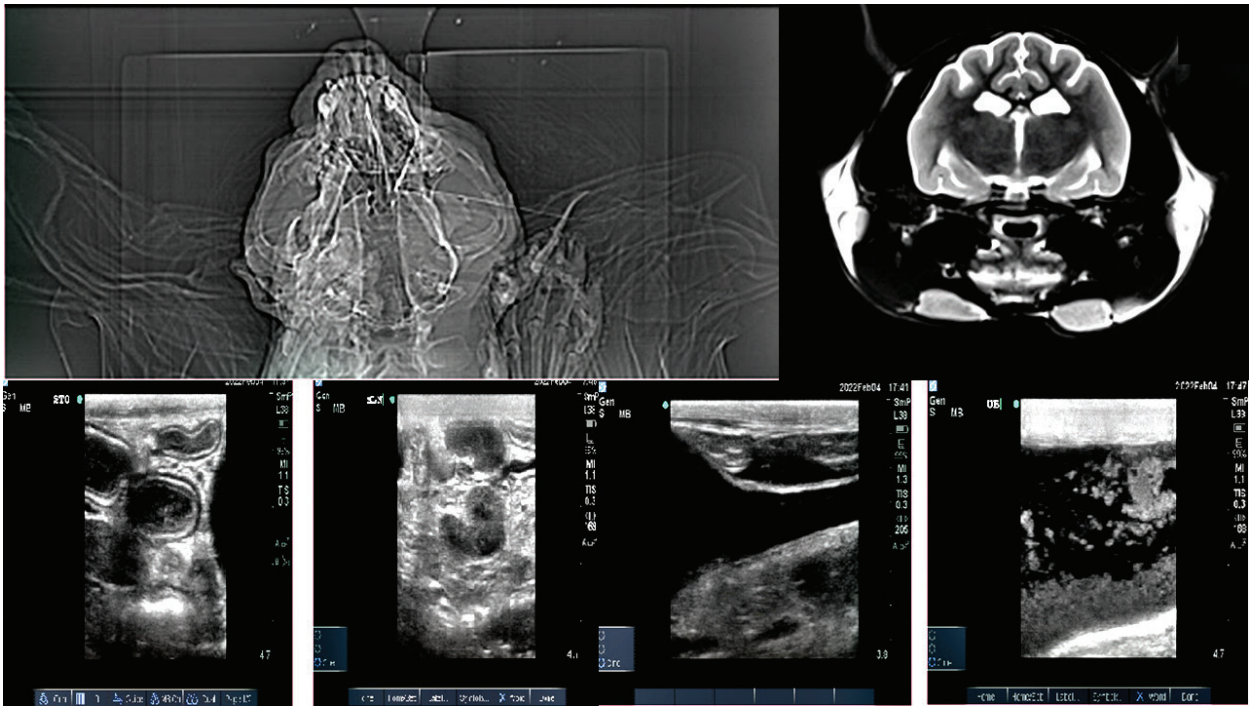


Fig. 2. Diagnostic imaging findings. (A) Brain computed tomography with enhanced meninges and choroid plexus. (B) Abdominal ultrasound showing hepatomegaly, splenomegaly, and enlarged mesenteric lymph nodes. (C) Sediment in the urinary bladder and mild abdominal effusion.

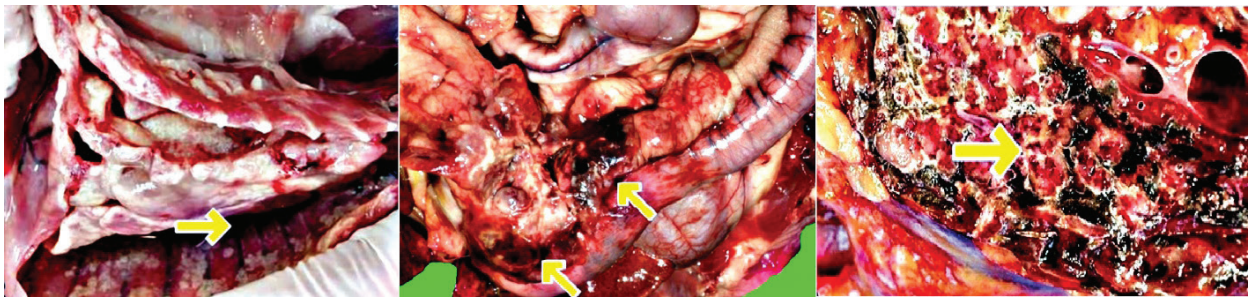


Fig. 3. Gross necropsy findings. Multiple small white fibrinous plaques (2–4 mm) were observed the serosal surfaces of the thoracic and abdominal organs, with evident icterus in the visceral and subcutaneous adipose tissue.

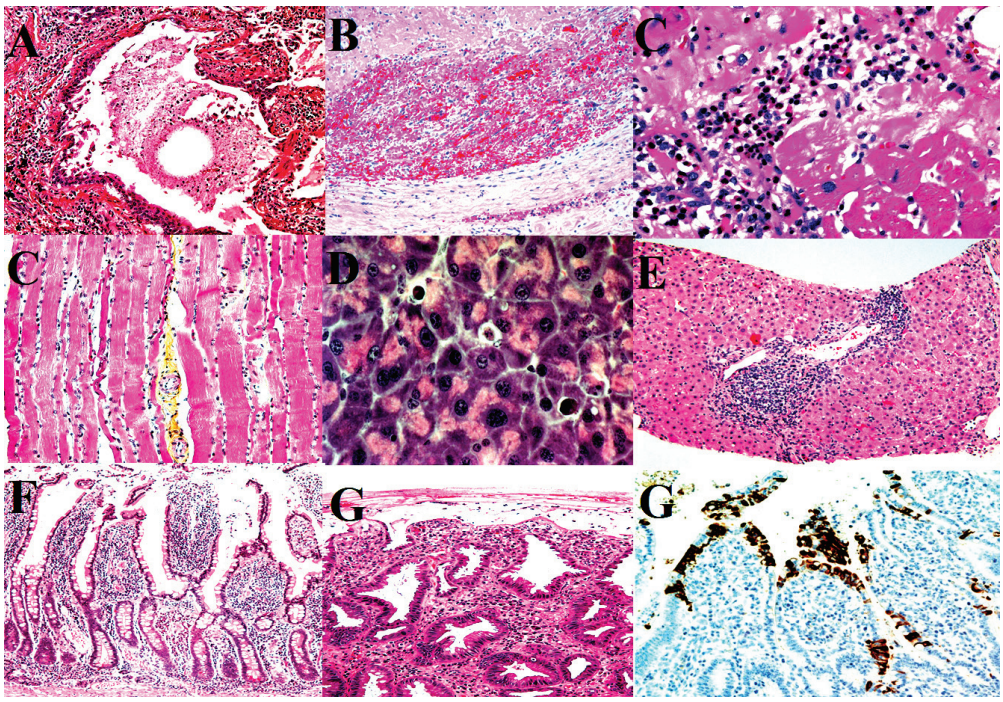


Fig. 4. Histopathological findings in the lung, heart, liver, and gastrointestinal tract. (A-B) Severe pulmonary edema, hyaline membranes, and vascular thrombosis. (A) Histiocytic, neutrophilic, and lymphoplasmacytic inflammation with multifocal areas of subserosal necrosis with varying degrees. (B) Vascular thrombosis, fibrinoid vasculitis, and syncytial cells. (C–D) Lymphoplasmacytic myocarditis with myocyte degeneration. (C) Hypereosinophilic myocytes and striations. (D) Single apoptotic hepatocyte (600X). (E) Interface hepatitis (piecemeal necrosis), death of hepatocytes at the interface of the parenchyma and connective tissue of the portal zone, accompanied by a variable degree of inflammation and fibrosis. (F–G) Gastric inflammation with neutrophilic vascular aggregates. (F) Jejunum, shortening and loss of epithelial cells with villus fusion and cellular debris along with moderate, multifocal, lympho-plasmacytic-histiocytic inflammation. (G) Ischemia-type colitis showing mucus depletion, patchy atrophic degeneration, polymorphonuclear neutrophil infiltration, and feline coronavirus spike protein in enterocytes and intestinal absorptive cells (Immunohistochemistry, Alkaline Phosphatase (AP), 1000X).

and subthalamic nucleus. Mild HS. Mononuclear perivascular inflammation. Fibrinoid necrosis of the vessel walls transtentorial herniation of the temporal uncus Acute ischemic hemorrhagic infarction within the middle meningeal artery territory (Fig. 6A–D). Severe viral-associated vasculitis and ischemic injury are reflected in the neuropathological changes.

Kidneys

Renal pathology was characterized predominantly by acute tubular injury, focal visceral epithelial hypercellularity consistent with collapsing glomerulopathy, and mild TMA. The tubular lumina contained proteinaceous casts, and the interstitial infiltration of mononuclear and neutrophilic inflammatory cells was observed (Fig. 6E). Renal changes indicate a septic-embolic insult and microvascular injury.

Eyes

Ocular lesions were prominent in the cornea, choroidal vasculature, and retina. The corneal pathology included inflammatory deposits on the endothelium and bilateral endothelial cell loss with Descemet's membrane thickening, indicative of endothelial failure. Retinal abnormalities included hemorrhages, horizontal focal central retinal degeneration microvascular lesions, and extensive retinal gliosis. The choroidal vasculature exhibited increased vessel density and intense inflammatory infiltration (Fig. 6F). The ocular pathology was consistent with end-stage uveitis and vasculitis (Carossino *et al.*, 2022).

Ethical approval

All necropsy and sampling procedures were approved by the Ethics Committee of Islamic Azad University, Sanandaj Branch (IR.IAU.SDJ.REC.1402.118, approved on August 27, 2024).

Discussion

This report presents the first molecularly and pathologically confirmed case of FIP in a captive Persian leopard (*Panthera pardus tulliana*),

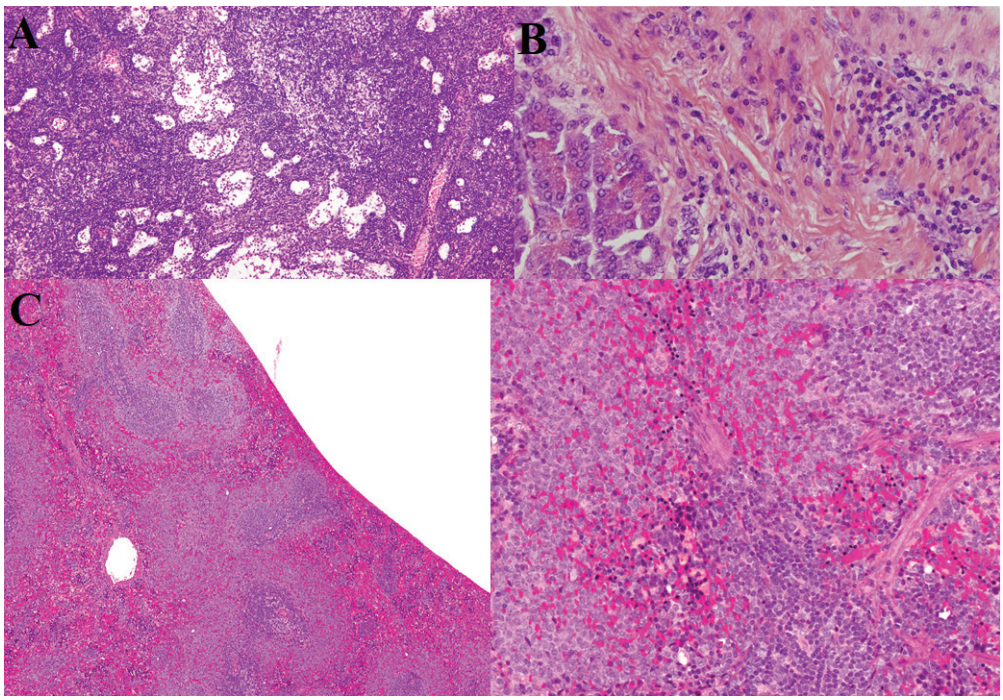


Fig. 5. Histopathology of lymphoid tissues, pancreas, and spleen. (A) Extensive necrosis, vascular thrombosis, cellular debris, lymphoid follicle depletion, and polymorphonuclear neutrophil infiltration. (B) Areas of inflammatory infiltration in the pancreas (hematoxylin and eosin staining, 400X). (C) Depletion of lymphoid follicles in the spleen and reduction of lymphocytes (hematoxylin and eosin staining, 300 dpi).

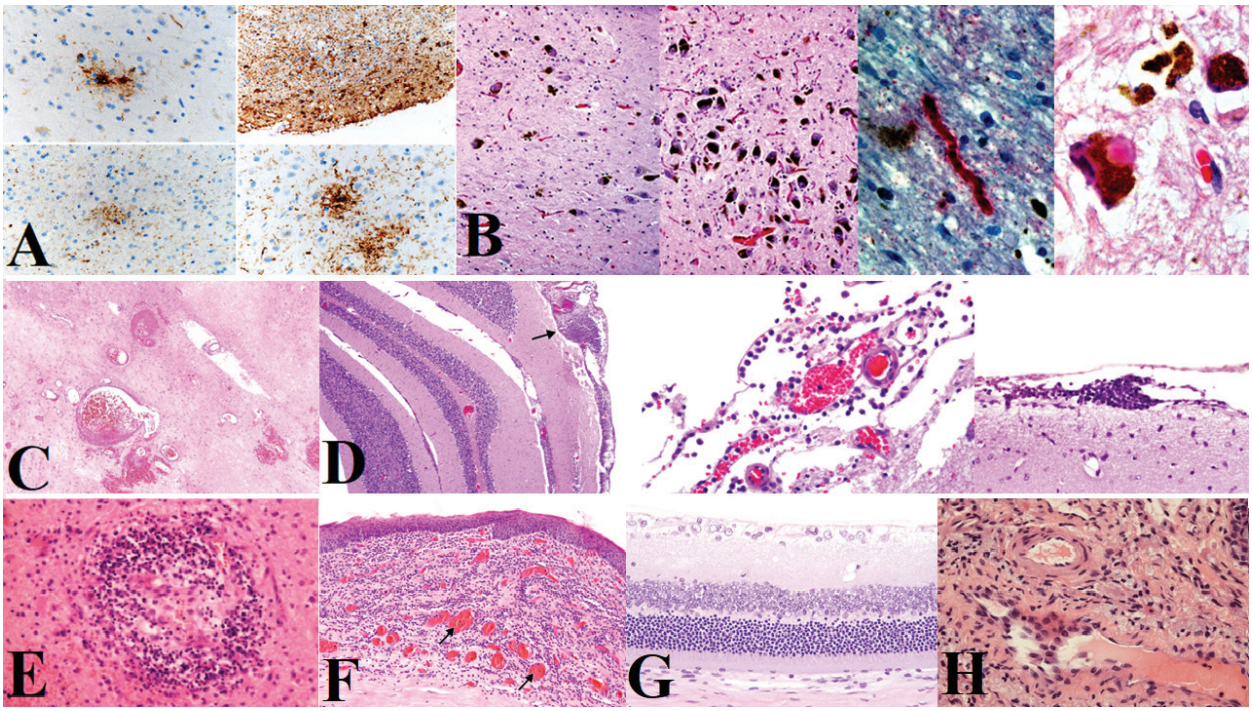


Fig. 6. Neuropathology and ocular lesions. (A and B) Thorn-shaped astrocytes and pallido-nigral degeneration. (C and D) Vascular necrosis, leptomeningeal inflammation, and perivascular lymphocytic infiltration. (E–H) Corneal inflammation, retinal degeneration, and choroidal vasculitis.

highlighting a significant conservation threat for this endangered subspecies. This case underscores the diagnostic challenges and therapeutic limitations of FIP in non-domestic felids (Paltrinieri *et al.*, 2021). Similar to previous reports in other large felids, such as tigers and cheetahs (Kennedy *et al.*, 2002; Stout *et al.*, 2021; Gaffney *et al.*, 2022). this case demonstrated characteristic systemic vasculitis, pyogranulomatous inflammation, and lymphoid depletion. However, the prominent neurotropic and ocular manifestations observed here, including thorn-shaped astrocytes and retinal vasculitis, represent a particularly severe disease phenotype, potentially reflecting species-specific susceptibility or viral factors. The proposed transmission route via predation of an FCoV-infected domestic cat remains plausible but unconfirmed, as the remains were not available for testing (Addie *et al.*, 2009). This hypothesis underscores the need for strict biosecurity measures in facilities housing endangered felids, particularly in regions where contact with domestic species may occur (Addie *et al.*, 2023). Despite initiating an antiviral regimen (GS-441524) and immunomodulatory therapy that has shown efficacy in domestic cats (Černá *et al.*, 2022a), the leopard exhibited rapid clinical deterioration and succumbed to the disease. This outcome highlights potential differences in disease progression or therapeutic response between domestic and non-domestic felids, possibly influenced by host genetics, stress, or delayed diagnosis. The adjunct use of corticosteroids, though intended to mitigate inflammation, may have adversely affected the outcome, as immunosuppression is generally contraindicated in FIP management (Černá *et al.*, 2022b). histopathological and molecular findings provide conclusive evidence of FIPV-induced multisystemic injury, with immune-complex-mediated vasculitis as the central pathogenic mechanism. Extensive adrenal hemorrhagic necrosis, which is consistent with Waterhouse–Friderichsen syndrome, further emphasizes the acute septicemic nature of the terminal disease in this case.

Study limitations

The single-case design limits this study. The absence of comprehensive FCoV screening of other felids in the facility or surrounding domestic cat populations prevents definitive conclusions about transmission dynamics. The animal's status and welfare considerations also constrained therapeutic monitoring.

Conclusion

This case underscores the vulnerability of endangered Persian leopards to fatal FIP and emphasizes the need proactive FCoV surveillance in captive breeding programs (Spada *et al.*, 2021). Early detection through routine fecal screening and molecular testing, coupled with stringent biosecurity measures prevent contact with potential domestic reservoirs, is essential for mitigating this threat within the One Health framework (Mohebali *et al.*, 2022).

Acknowledgments

The authors would like to thank the wildlife veterinary and pathology team at Tehran Eram Zoo, especially Dr. P. Mohammadzadeh, for their clinical management and diagnostic imaging support. We also acknowledge the Environmental Toxicology Unit at Laleh Veterinary Laboratory for their guidance on endocrine biomarker analysis and the laboratory's assistance with sample processing and histopathology.

Conflict of interest

The authors have no competing financial or personal interests to declare.

Funding

This research received no specific funding from any granting agency.

Author contributions

Peyman Mohammadzadeh: Conceptualization, Methodology, Investigation, Formal analysis, Original Draft Writing, Review & Editing, Visualization, Project administration.

Farshad Ziaee: Investigation, Data Curation, Formal Analysis, Writing, Review, and Editing.

Farnoush Mousavi: Investigation, Data Curation, Formal analysis, Writing, Review, and Editing.

Data availability

The data generated during this study contain sensitive information and are not publicly available. Reasonable requests for data access should be directed to the corresponding author.

References

Addie, D., Houe, L., Maitland, K., Passantino, G. and Decaro, N. 2020. Cat litters and FCoV. J. Feline Med. Surg. 22(4), 350–357.

Addie, D., Belák, S., Boucraut-Baralon, C., Egberink, H., Frymus, T., Gruffydd-Jones, T., Hartmann, K., Hosie, M.J., Lloret, A., Lutz, H. and Marsilio, F. 2009. FIP ABCD guidelines. J. Feline Med. Surg. 11(7), 594–604.

Addie , D.D., Bellini, F., Covell-Ritchie, J., Crowe, B., Curran, S., Fosbery, M., Hills, S., Johnson, E., Johnson, C., Lloyd, S. and Jarrett, O. 2023. Stopping feline coronavirus shedding prevented feline infectious peritonitis. Viruses 15(4), 222–229.

Altan, E., Delaney, M.A., Colegrove, K.M., Spraker, T.R., Wheeler, E.A., Deng, X., Li, Y., Gulland, F.M. and Delwart, E. 2020. Virome in sea lion lymph node. Viruses 12(8), 793.

Azadian, A. and Gunn-Moore, D.A. 2022. Age-related cognitive impairments in domestic cats naturally infected with feline immunodeficiency virus. Vet. Record 191(1), e1683.

Barrs, V.R., Peiris, M., Tam, K.W., Law, P.Y., Brackman, C.J., To, E.M., Yu, V.Y., Chu, D.K., Perera, R.A.

and Sit, T.H. 2020. SARS-CoV-2 in quarantined domestic cats from COVID-19 households, Hong Kong, China. Emerg. Infect. Dis. 26(12), 3071–3074.

Bartlett, S.L., Diel, D.G., Wang, L., Zec, S., Laverack, M., Martins, M., Caserta, L.C., Killian, M.L., Terio, K., Olmstead, C. and Delaney, M.A. 2021. SARS-CoV-2 infection and longitudinal fecal screening in Malayan tigers, Amur tigers, and African lions at the Bronx Zoo. J. Zoo Wildlife Med. 51(4), 733–744.

Böger, B., Fachi, M.M., Vilhena, R.O., Cobre, A.F., Tonin, F.S. and Pontarolo, R. 2021. COVID-19 diagnostic tests meta-analysis. Am. J. Infect. Control 49(1), 21–29.

Carossino, M., Del Piero, F., Lee, J., Needle, D.B., Levine, J.M., Riis, R.R., Maes, R., Wise, A.G., Mullaney, K., Ferracone, J. and Langohr, I.M. 2022. Uveal inflammation in FIP. Pathogens 11(8), 883.

Černá, P., Ayoob, A., Baylor, C., Champagne, E., Hazanow, S., Heidel, R.E., Wirth, K., Legendre, A.M. and Gunn-Moore, D.A. 2022. Polyprenyl immunostimulant in FIP. Pathogens 11(8), 881.

Černá, P., Lobová, D., Bubeníková, J., Vrábelová, J., Molínková, D. and Hořín, P. 2022. FCoV shedding patterns in catteries. Res. Vet. Sci. 152, 524–529.

Collier, A.R.Y., Yu, J., McMahan, K., Liu, J., Atyeo, C., Ansel, J.L., Fricker, Z.P., Pavlakis, M., Curry, M.P., Jacob-Dolan, C. and Patel, H. 2021. COVID-19 mRNA vaccines in pregnancy. JAMA 325(23), 2370–2380.

Duan, L., Zheng, Q., Zhang, H., Niu, Y., Lou, Y. and Wang, H. 2020. SARS-CoV-2 spike glycoprotein. Front. Immunol. 11, 576622.

Felten, S. and Hartmann, K. 2019. FIP diagnosis review. Viruses 11(11), 1068.

Gaffney, P.M., Kennedy, M., Terio, K., Gardner, I., Lothamer, C., Coleman, K. and Munson, L. 2022. FCoV in cheetah feces. J Zoo Wildlife Med. 43(4), 776–786.

Gao, Y.Y., Liang, X.Y., Wang, Q., Zhang, S., Zhao, H., Wang, K., Hu, G.X., Liu, W.J. and Gao, F.S. 2022. Feline coronavirus comparison. Gene 825, 146443.

Giselbrecht, J., Bergmann, M., Hofmann-Lehmann, R. and Hartmann, K. 2022. FeLV infection diagnosis. Tierärztliche Praxis Ausgabe K: Kleintiere/Heimtiere 50(3), 198–212.

Guimaraes, A.M., Brandão, P.E., de Moraes, W., Cubas, Z.S., Santos, L.C., Villarreal, L.Y., Robes, R.R., Coelho, F.M., Resende, M., Santos, R.C., Oliveira, R.C., Yamaguti, M., Marques, L.M., Neto, R.L., Buzinhani, M., Marques, R., Messick, J.B., Biondo, A.W. and Timenetsky, J. 2009. FeLV and FCoV in wild felids. J. Zoo Wildlife Med. 40(2), 360–364.

Hohdatsu, T., Okada, S. and Koyama, H. 1991. Monoclonal antibodies against FIPV. Arch. Virol. 117(1-2), 85–95.

Junqueira, C., Crespo, Â., Ranjbar, S., de Lacerda, L.B., Lewandrowski, M., Ingber, J., Parry, B., Ravid, S., Clark, S., Schrimpf, M.R., Ho, F., Beakes, C., Margolin, J., Russell, N., Kays, K., Boucau, J., Das Adhikari, U., Vora, S.M., Leger, V., Gehrke, L. and Lieberman, J. 2022. FcγR-mediated SARS-CoV-2 infection. Nature 606(7914), 576–584.

Kennedy, M., Citino, S., McNabb, A.H., Moffatt, A.S., Gertz, K. and Kania, S. 2002. FCoV in captive Felidae. J. Vet. Diagn. Invest. 14(6), 520–522.

Kennedy, M.A. 2020. Feline infectious peritonitis update. Vet. Clin. North Am. Small Anim Pract 50(5), 1001–1011.

Klaus, J., Palizzotto, C., Zini, E., Meli, M.L., Leo, C., Egberink, H., Zhao, S. and Hofmann-Lehmann, R. 2021. SARS-CoV-2 infection and antibody response in a symptomatic cat from Italy with intestinal B-cell lymphoma. Viruses 13(3), 527.

Lin, L., Yao, D., Wu, L., Fan, R., Liu, Y. and Zhou, Z. 2022. Molecular epidemiology of feline coronavirus in China. Arch. Virol. 167(1), 189–194.

McAloose, D., Laverack, M., Wang, L., Killian, M.L., Caserta, L.C., Yuan, F., Mitchell, P.K., Queen, K., Mauldin, M.R., Cronk, B.D., Bartlett, S.L., Sykes, J.M., Zec, S., Stokol, T., Ingerman, K., Delaney, M.A., Fredrickson, R., Ivančić, M., Jenkins-Moore, M., Mozingo, K. and Diel, D.G. 2020. SARS-CoV-2 in tigers and lions. mBio 11(5), e02220–e02220.

Michael, H.T., Waterhouse, T., Estrada, M. and Seguin, M.A. 2021. Frequency of respiratory pathogens and SARS-CoV-2 in canine and feline samples. J. Small Anim. Pract. 62(5), 336–342.

Mohebali, M., Hassanpour, G., Zainali, M., Gouya, M.M., Khayatzadeh, S., Parsaei, M., Sarafraz, N., Hassanzadeh, M., Azarm, A., Salehi-Vaziri, M., Sasani, F., Heidari, Z., Jalali, T., Pouriayevali, M.H., Shoja, Z., Ahmadi, Z., Sadjadi, M., Tavakoli, M., Azad-Manjiri, S., Karami, C. and Zarei, Z. 2022. SARS-CoV-2 in domestic cats in northwest Iran. Virus Res. 310, 198673.

Newman, A., Smith, D., Ghai, R.R., Wallace, R.M., Torchetti, M.K., Loiacono, C., Murrell, L.S., Carpenter, A., Moroff, S., Rooney, J.A. and Barton Behravesh, C. 2020. First reported cases of SARS-CoV-2 infection in companion animals—New York, March-April 2020. MMWR 69(23), 710–713.

Paltrinieri, S., Giordano, A., Stranieri, A. and Lauzi, S. 2021. FIP and COVID-19 similarities. Transboundary Emerg. Dis. 68(4), 1786–1799.

Pedersen, N.C. 1987. FIP virology and immunology. Adv. Exp. Med. Biol. 218, 529–550.

Pérez-González, J., Carranza, J., Martínez, R. and Benítez-Medina, J.M. 2021. Host genetic diversity and infectious diseases, Focus on wild boar, red deer and tuberculosis. Animals 11(6), 1630.

Rottier, P.J. 1999. Molecular dynamics of feline coronaviruses. Vet. Microbiol. 69(1-2), 117–125.

Scaglione, F.E., Biolatti, C., Pregel, P., Berio, E., Cannizzo, F.T., Biolatti, B. and Bollo, E. 2019. Zoo mortality survey. PeerJ 7, e6198.

Shyr, Z.A., Cheng, Y.S., Lo, D.C. and Zheng, W. 2021. Drug combination therapy. Drug Discov Today 26(10), 2367–2376.

Sila, T., Sunghan, J., Laochareonsuk, W., Surasombatpattana, S., Kongkamol, C., Ingviya, T., Siripaitoon, P., Kositpantawong, N., Kanchanasuwan, S., Hortiwakul, T., Charernmak, B., Nwabor, O.F., Silpapojakul, K. and Chusri, S. 2022. Suspected cat-to-human transmission of SARS-CoV-2, Thailand. Emerg. Infect. Dis. 28(7), 1485–1488.

Simons, F.A., Vennema, H., Rofina, J.E., Pol, J.M., Horzinek, M.C., Rottier, P.J. and Egberink, H.F. 2005. mRNA PCR for FIP diagnosis. J. Virol. Methods 124(1-2), 111–116.

Spada, E., Vitale, F., Bruno, F., Castelli, G., Reale, S., Perego, R., Baggiani, L. and Proverbio, D. 2021. SARS-CoV-2 infection in stray cats from northern Italy. Viruses 13(4), 618.

Stout, A.E., André, N.M. and Whittaker, G.R. 2021. FIP in non-domestic felids. J. Zoo Wildlife Med. 52(1), 14–27.

Stranieri, A., Scavone, D., Paltrinieri, S., Giordano, A., Bonsembiante, F., Ferro, S., Gelain, M.E., Meazzi, S. and Lauzi, S. 2020. FIP diagnostic concordance. Pathogens 9(10), 852.

Takeda, M. 2022. Proteolytic activation of SARS-CoV-2 spike. Microbiol. Immunol. 66(1), 15–23.

Tortorici, M.A., Czudnochowski, N., Starr, T.N., Marzi, R., Walls, A.C., Zatta, F., Bowen, J.E., Jaconi, S., Di Iulio, J., Wang, Z., De Marco, A., Zepeda, S.K., Pinto, D., Liu, Z., Beltramello, M., Bartha, I., Housley, M.P., Lempp, F.A., Rosen, L.E., Dellota, E. Jr. and Pizzuto, M.S. 2021. Broad sarbecovirus neutralization by human antibody. Nature 597(7874), 103–108.

Tortorici, M.A., Walls, A.C., Joshi, A., Park, Y.J., Eguia, R.T., Miranda, M.C., Kepl, E., Dosey, A., Stevens-Ayers, T., Boeckh, M.J., Telenti, A., Lanzavecchia, A., King, N.P., Corti, D., Bloom, J.D. and Veesler, D. 2022. Structure of human coronavirus spike. Cell 185(13), 2279–2291.

Van Rensburg, I.B. and Silkstone, M.A. 1984. Concomitant FIP and toxoplasmosis in a cheetah. J. South Afr. Vet. Assoc. 55(4), 205–207.

Vuong, W., Khan, M.B., Fischer, C., Arutyunova, E., Lamer, T., Shields, J., Saffran, H.A., McKay, R.T., van Belkum, M.J., Joyce, M.A., Young, H.S., Tyrrell, D.L., Vederas, J.C. and Lemieux, M.J. 2020. Feline coronavirus drug inhibits SARS-CoV-2 protease. Nat. Commun. 11(1), 4282.

Wang, G., Hu, G., Liang, R., Shi, J., Qiu, X., Yang, Y., Jiao, Z., Chen, Y., Shen, Z., Li, M., Shi, Y., Mao, J. and Peng, G. 2021. Feline coronavirus infection model. J. Virol. 95(21), e00745–e00721.

Wen, W., Chen, C., Tang, J., Wang, C., Zhou, M., Cheng, Y., Zhou, X., Wu, Q., Zhang, X., Feng, Z., Wang, M. and Mao, Q. 2022. Oral antivirals for COVID-19 meta-analysis. Ann. Med. 54(1), 516–523.

Woods, R.D. 2022. Enteric coronaviruses in feline cells. Vet. Microbiol. 7(5), 427–435.

Yin, Y., Li, T., Wang, C., Liu, X., Ouyang, H., Ji, W., Liu, J., Liao, X., Li, J. and Hu, C. 2021. Clinical features of feline infectious peritonitis in Wuhan, China. Sci. Rep. 11(1), 5208.

Supplementary materials

S1. Detailed anesthesia and sample collection protocol
Chemical immobilization was achieved (Supplementary Material S1) using a combination of ketamine hydrochloride (Ketamine 10%, Alfasan, Netherlands; 2.5–3 mg/kg) and medetomidine hydrochloride (Medetomidine 0.1%, Virbac, France; 0.05–0.07 mg/kg) administered intramuscularly via remote darting. Anesthesia was reversed with atipamezole hydrochloride (Antisedan, Orion Pharma, Finland; 0.3–0.35 mg/kg), administered 25% intravenously and 75% subcutaneously. Blood samples were collected aseptically from the right jugular vein using a 20G needle. Approximately 10 ml of blood was drawn into EDTA tubes (BD Vacutainer, USA) and serum separator tubes (BD Vacutainer, USA). EDTA samples were centrifuged at 3,500 rpm for 12 minutes (Centrifuge 5804 R, Eppendorf, Germany) within 30 minutes of collection. Plasma and serum aliquots were stored at –25°C and –80°C, respectively, pending analysis.

S2. Molecular diagnostics detailed methodsRNA extraction
Viral RNA was extracted from 200 µl of plasma using the QIAamp Viral RNA Mini Kit (Qiagen, Germany; Cat. No. 52906) according to the manufacturer›s instructions.

RT-PCR: Reverse transcription polymerase chain reaction (RT-PCR) was performed using the OneStep RT-PCR Kit (Qiagen, Germany; Cat. No. 210212). The 25 µl reaction mixture contained 5 µl of extracted RNA, 12.5 µl of 2x RT-PCR Buffer, 1 µl of enzyme mix, and 10 pmol of each primer. The primers targeting the FCoV membrane (M) gene (forward: 5′-CAT TAC TAC TAC CAT GAC TAC-3′; reverse: 5′-CAT ATC ATA GAC ATC ATA TCA-3′) and leader sequence (forward: 5′-GCT ATT ACA GAC CAT TAC AC-3′; reverse: 5′-CTA TCA TAG CCA TAC ATA C-3′) were adopted from Stranieri *et al.* (2020) and Hohdatsu *et al.* (1991). Thermal cycling conditions were: 50°C for 30 minutes (reverse transcription); 95°C for 15 minutes (initial denaturation); followed by 40 cycles of 94°C for 30 seconds, 55°C for 30 seconds, and 72°C for 1 minute; with a final extension at 72°C for 10 minutes. Amplicons were visualized on a 1.5% agarose gel.

Reference strains: The following reference strains were propagated in *Felis catus* whole fetus (fcwf-4) cells (ATCC® CRL-2787™) or feline embryonic lung (FEL) cells: FIPV WSU-79-1146 (ATCC® VR-2202™), FIPV type II 79-1683, FIPV UCD2, FIPV UCD4, and FECV UCD. Propagation and RNA extraction from reference strains followed established protocols (Woods, 1982; Woods, 2022).

S3. Detailed immunohistochemistry (IHC) and *in situ* hybridization (ISH) protocols IHC protocol
Formalin-fixed paraffin-embedded (FFPE) tissue sections (4 µm) were deparaffinized and rehydrated. For CD68 and cleaved caspase-3 detection, heat-induced epitope retrieval was performed in citrate buffer (pH 6.0) using a microwave. For ACE2, enzymatic retrieval with Proteinase K (Dako, Denmark; Cat. No. S3020) was used. Endogenous peroxidase activity was blocked with 3% H_2O_2. Sections were incubated with primary antibodies for 60 minutes at room temperature: monoclonal mouse anti-CD68 (1:50, clone KP1, Dako, Cat. No. M0814), rabbit anti-cleaved caspase-3 (1:60, Cell Signaling Technology, USA; Cat. No. 9661), and rabbit anti-ACE2 (1:500, Abcam, UK; Cat. No. ab15348). Detection was performed using the LSAB+ System-HRP (Dako, Cat. No. K0690) for CD68 and ACE2, and an alkaline phosphatase-conjugated system (Vector Laboratories, USA; Cat. No. AK-5200) for caspase-3, with DAB (Dako, Cat. No. K3468) or Fast Red (Vector Laboratories, Cat. No. SK-5100) as chromogens, respectively. Sections were counterstained with Mayer›s hematoxylin.

ISH Protocol: RNAscope ISH was performed using the RNAscope 2.5 HD Assay-RED (ACD/Bio-Techne, USA; Cat. No. 322350) according to the manufacturer›s instructions. The FIPV-specific spike gene probe (V-NCoV2019-S, ACD/Bio-Techne; Cat. No. 848561) was used. RNA integrity was confirmed using a Macaca mulatta UBC positive control probe (ACD/Bio-Techne; Cat. No. 310771). Signal was detected using Fast Red chromogen.

S4. Detailed pharmacological agents and treatment protocol GS-441524
Administered subcutaneously at a concentration of 16 mg/ml (SAK 441524™, SAK Pharmaceuticals, Netherlands; Batch No. 220115). Dosage was calculated at 4 mg/kg every 24 hours for 23 days.

Polyprenyl Immunostimulant: Administered orally at 0.25 ml/kg twice daily (VetImmune®, VPL, USA; Batch No. 211209) for 15 days.

Glucocorticoids: Prednisolone sodium succinate (Prednisolone 10%, Vetoquinol, India; Batch No. 220304) was administered intramuscularly at ~10 mg/kg once daily for 3 days, followed by a tapering regimen of oral prednisolone (<2 mg/kg/day).

S5. Necropsy protocol compliance
Necropsy was performed in strict adherence to the *EAZA Husbandry Guidelines for the Leopard (Panthera pardus spp.)*, 1st Edition (September 2009), and the *Snow Leopard SSP Gross Necropsy Protocol* (AZA Animal Health Committee and Veterinary Scientific Advisory Group, December 2023). All organ systems were examined systematically. Tissue samples for histopathology were fixed in 10% neutral buffered formalin for 48 hours. Samples for molecular diagnostics were flash-frozen in liquid nitrogen and stored at –80°C.